Supplement of Hydrol. Earth Syst. Sci., 29, 547–566, 2025
https://doi.org/10.5194/hess-29-547-2025-supplement

Hydrology and Earth System Sciences
Open Access
EGU

Supplement of

Do land models miss key soil hydrological processes controlling soil moisture memory?

Mohammad A. Farmani et al.

Correspondence to: Mohammad A. Farmani (farmani@arizona.edu) and Guo-Yue Niu (niug@arizona.edu)

S1. Detailed Descriptions of Equations and Parameters of the Noah-MP Model Used in This Study

To provide a comprehensive view of the soil moisture simulations, we summarize the core equations from Niu et al. (2011). Below, we detail the primary processes involved in soil moisture dynamics in the custom Noah-MP model:

S1.1. Mass-Based and Mixed-Form Richards Equation (RE)

Noah-MP solves the mass-based (or θ-based) Richards Equation (RE) for liquid water flow (Niu et al., 2011), represented as:

$$\frac{\partial \theta_{liq}}{\partial t} = \frac{\partial}{\partial z}\left[D\left(\frac{\partial \theta_{liq}}{\partial z}\right) + K\right] \tag{S1}$$

$$D = K(\theta)\frac{dh}{d\theta} \tag{S2}$$

Here, θ_{liq} is the volumetric liquid soil content [m^3/m^3], D [m^2/s] is diffusivity, and K [m/s] is hydraulic conductivity calculated using the Brooks and Corey (1964) model:

$$K = \left(1 - F_{frz}\right)K_s\left(\frac{\theta}{\theta_s}\right)^{2b+3} \tag{S3}$$

$$h = h_s\left(\frac{\theta}{\theta_s}\right)^{-b} \tag{S4}$$

Mixed-Form RE (Celia et al., 1990) addresses both water content and pressure head dynamics, providing an adaptable approach that allows for perfect mass balance. The mixed form applied here is:

$$\frac{\partial \theta_{liq}}{\partial t} = \frac{\partial}{\partial z}\left[K\left(\frac{\partial h}{\partial z} + 1\right)\right] \tag{S5}$$

Niu et al. (2024) implemented two optional soil hydraulics models: van Genuchten-Mualem (vGM) (Mualem, 1976; van Genuchten, 1980) and Brooks and Corey (1964). For the vGM model, the hydraulic conductivity takes the form of:

$$K = K_s s^{0.5}\left[1 - \left(1 - s^{1/m}\right)^m\right]^2, \tag{S6}$$

where *s* (-) is the relative saturation (van Genuchten, 1980):

$$s = \frac{\theta_{liq} - \theta_r}{\theta_e - \theta_r} = (1 + |\alpha h|^n)^{-m}. \tag{S7}$$

In equations (S6) and (S7), *n* (-) is the water retention curve parameter, $m = 1 - 1/n$, $\theta_e = \theta_s - \theta_{ice}$, is the effective porosity, θ_r is the residual soil moisture, and α (m^{-1}) is inverse of the air entry pressure. Another option takes the form of Brooks and Corey (1964), which is modified for frozen conditions:

$$K = (1 - F_{frz})K_s \left(\frac{\theta_{liq}}{\theta_s - \theta_{ice}}\right)^{2b+3} \quad \text{(S8)}$$

$$h = h_s \left(\frac{\theta_{liq}}{\theta_s - \theta_{ice}}\right)^{-b}. \quad \text{(S9)}$$

S1.2. Atmospheric Boundary Conditions, Surface Ponding, and Infiltration-Excess Runoff

The atmospheric (upper) boundary conditions in the model shift between head (Dirichlet) and flux (Neumann) conditions following Paniconi et al. (1994). When the surface pressure head exceeds the air entry pressure, flux boundaries are converted to head conditions, leading to surface ponding. Ponding depth, H_{top}^{t+1} (m), at each timestep is computed as:

$$H_{top}^{t+1} = H_{top}^{t} + (I_{pot} - I_{act})\Delta t_{fine} \quad \text{(S10)}$$

- Here, $I_{pot} = Q_s - R_{sat} - E_{soil}$ represents potential infiltration, where Q_s (m/s) is the incident surface water, R_{sat} (m/s) is saturation excess runoff calculated with the TOPMODEL approach (Niu et al., 2005), and E_{soil} (m/s) is soil evaporation. Actual infiltration, I_{act} (m/s), is diagnosed based on the balance of the water storage in the top layer:

$$I_{act} = \frac{\Delta\theta_1 \Delta z_1}{\Delta t_{fine}} + K_{1,2}\left(\frac{h_1 - h_2}{\Delta z_{1,2}} + 1\right) - Q_{ss,1} \quad \text{(S11)}$$

- Surface runoff R_{ex} (m/s) occurs when ponding depth exceeds a threshold $H_{top,max}$ (mm):

$$R_{ex} = max\left[0, (H_{top}^{t+1} - H_{top,max})\right]/\Delta t_{fine} \quad \text{(S12)}$$

S1.3. Dual Permeability Model (DPM)

The DPM integrates two domains (matrix and macropore) for capturing preferential flow:

$$\frac{\partial\theta_f}{\partial t} = \frac{\partial}{\partial z}\left[K_f(h_f)\left(\frac{\partial h_f}{\partial z} + 1\right)\right] - \frac{\Gamma_w}{F_f} \quad \text{(S13)}$$

$$\frac{\partial\theta_m}{\partial t} = \frac{\partial}{\partial z}\left[K_m(h_m)\left(\frac{\partial h_m}{\partial z} + 1\right)\right] + \frac{\Gamma_w}{1 - F_f} \quad \text{(S14)}$$

- where F_f is the ratio of the volume of the macropores to the total soil pore volume, Γ_w [1/m] is the transfer rate for water from the macropore domain to the micropore pore domain (or lateral infiltration). Γ_w is assumed to be proportional to the difference in pressure head between the two pore domains (Gerke and van Genuchten, 1993a):

$$\Gamma_w = \alpha_w (h_a - h_i), \quad \text{(S15)}$$

where α_w is a first-order mass transfer coefficient, depending on soil particle shape, diffusion pathlength (i.e., half the aggregate width), and the hydraulic conductivity at the matrix-macropore interface, K_{mf} (Šimůnek et al., 2003). It is simply parametrized in this study:

$$\alpha_w = 1\times 10^{-5}\,(1 - F_{frz})\,K_{mf}, \tag{S16}$$

where F_{frz} is the volumetric ice fraction. K_{fm} takes a harmonic mean of the those of the macropores, K_f, and matrix, K_m: $K_{mf} = 2\,K_f\,K_m\,/\,(\,K_f + K_m) \approx 2\,K_m$, when $K_f \ll K_m$, implying the water transfer between the two porous domains are mainly controlled by the hydraulic conductivity of matrix. Γ_w can be positive, representing diffusion of water flowing downward along the walls of macropores to surrounding drier matrix during infiltration, or negative, representing diffusion of water held in matrix to the drier walls of the macropores during dry-down periods. The water exchange between matrix and macropores at layer l, $Q_{ex,l} = \Gamma_{w,l}\Delta z_{,l}$ (m/s), is then added to the source/sink terms. Without this flux exchange, the water table depth in the matrix and macropore domains would be very different.

The model also represents flow of surface ponded water in the matrix domain, Q_{mf} [m/s], to the macropore domain at the Noah-MP time step. When the ponding depth over the matrix domain, $H_{top,m} > 0$, and the ponding depth over macropore domain, $H_{top,f} = 0$, Q_{mf} [m/s] is parameterized as:

$$Q_{mf} = 0.01 H_{top,m}/(\Delta t_{MP} F_f), \tag{S17}$$

and $H_{top,m}$ [m] is then updated:

$$H_{top,m} = H_{top,m} - 0.01 H_{top,m}/(1 - F_f). \tag{S18}$$

Q_{mf} is then added to the surface incident water in the macropore domain (Q_s). If $H_{top.m}$ and $H_{top,f}$ are both greater than 0, they are assumed the same: $H_{top,m} = H_{top,f} = H_{top}$, where $H_{top} = F_f\,H_{top,f} + (1-F_f)\,H_{top,m}$.

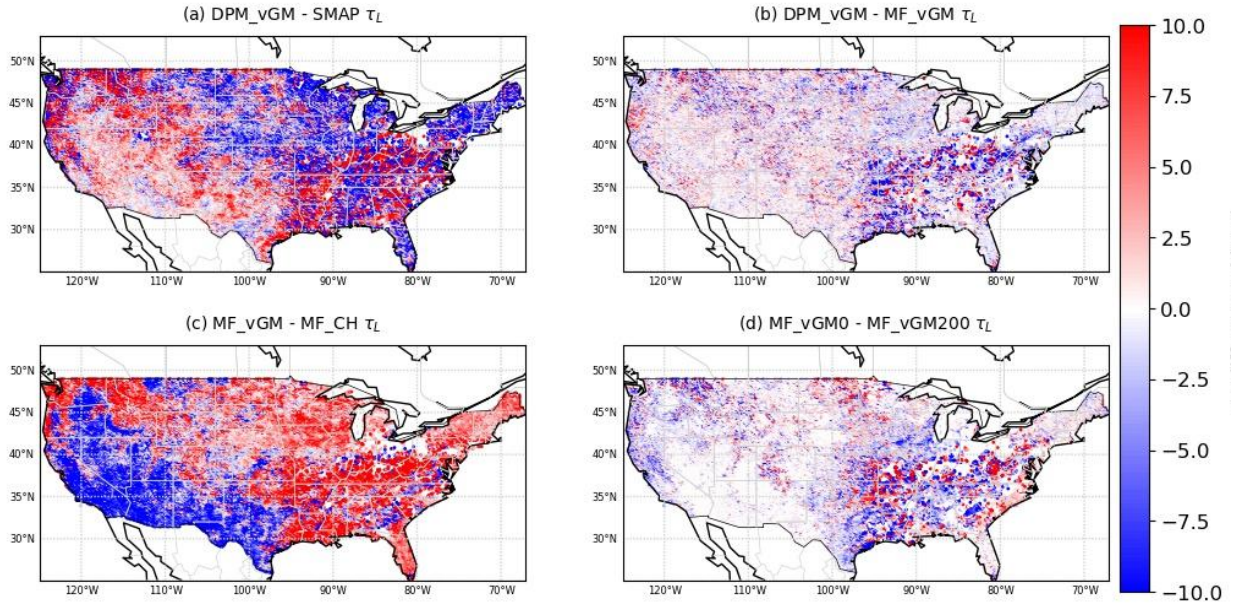

Figure S1 Spatial distribution of long-term memory differences (a) between the Dual-Permeability model and SMAP; (b) between the Dual-Permeability and Mixed-Richards models; (c) between the Mixed-Richards models using Van-Genuchten and Clapp-Hornberger parameterizations; and (d) between the Mixed-Richards models with zero and 200 mm ponding depths.

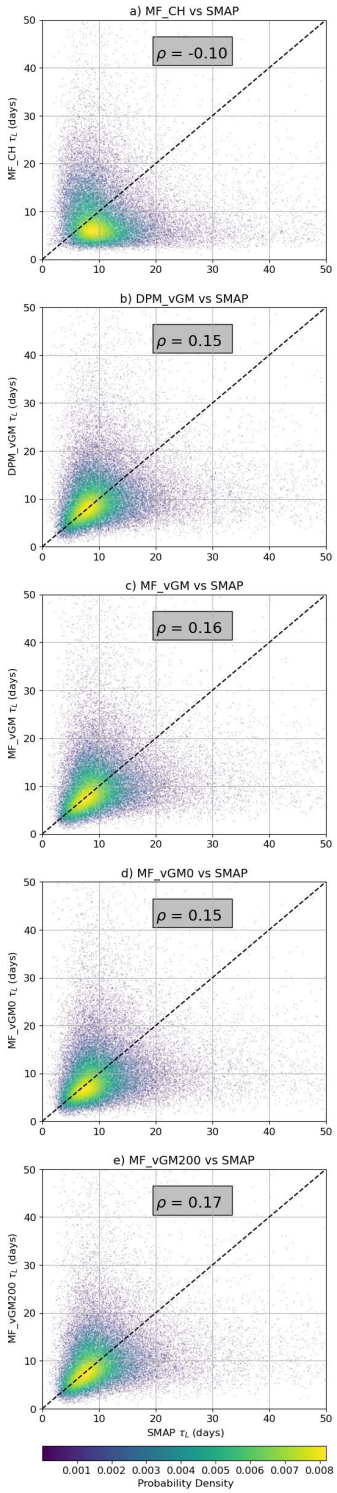

Figure S2 Scatterplot of root zone τ_L estimated from SMAP versus (a) MF_CH; (b) DMP_VGM; (c) MF_VGM; (d) MF_VGM0; and (e) MF_VGM200.

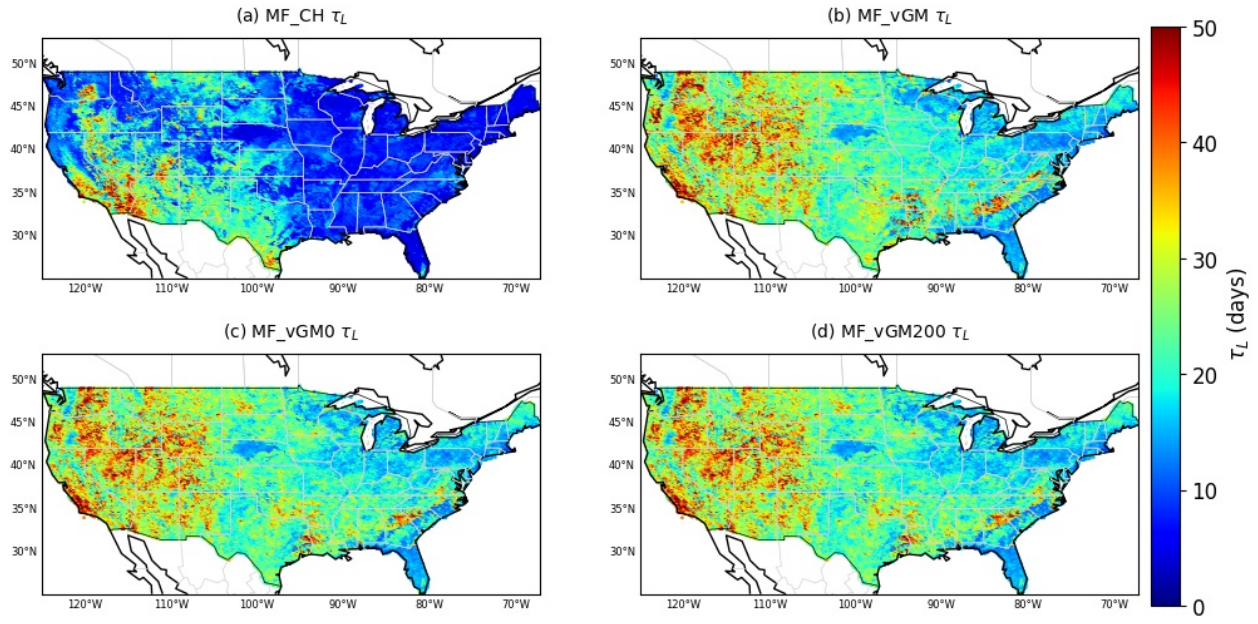

Figure S3 Spatial distribution of root zone $\tau_L$estimated from (a) MF_CH (b) MF_VGM; (c) MF_VGM0; and (d) MF_VGM200.

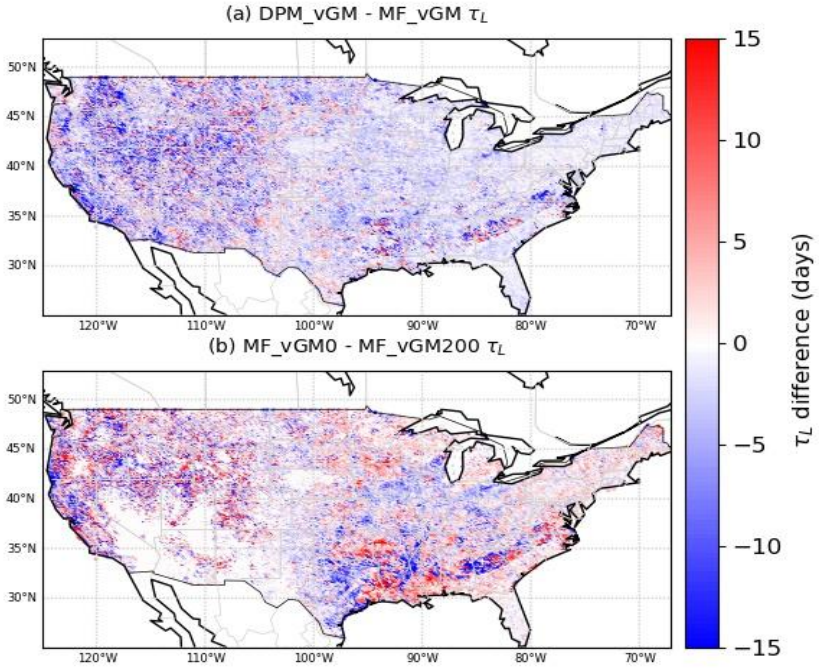

Figure S4 Spatial distribution of root zone long-term memory differences (a) between the Dual-Permeability and Mixed-Richards models; (b) within the Mixed-Richards models contrasting zero ponding depth to a 200 mm ponding depth.

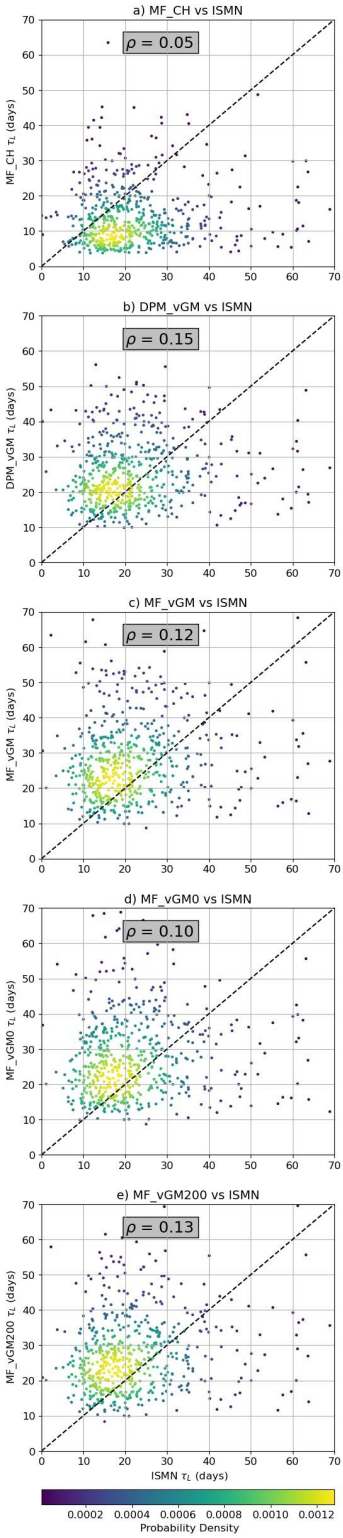

Figure S5 Scatterplot of root zone $\tau_L$estimated from SMAP versus (a) MF_CH; (b) DMP_VGM; (c) MF_VGM; (d) MF_VGM0; and (e) MF_VGM200.

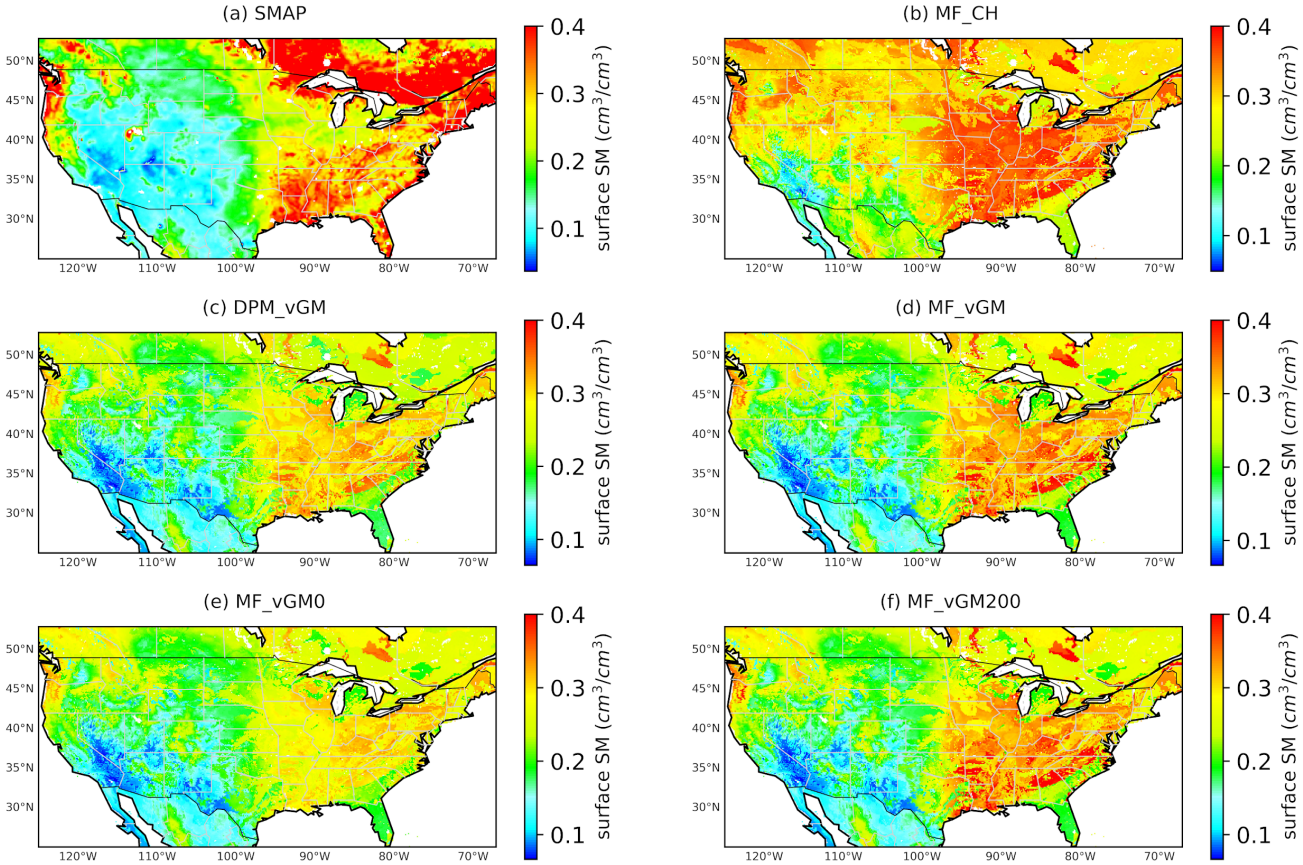

Figure S6 Average surface soil moisture over 2015−2019: (a) SMAP; (b) MF_CH; (c) DMP_VGM; (d) MF_VGM; (e) MF_VGM0; and (f) MF_VGM200

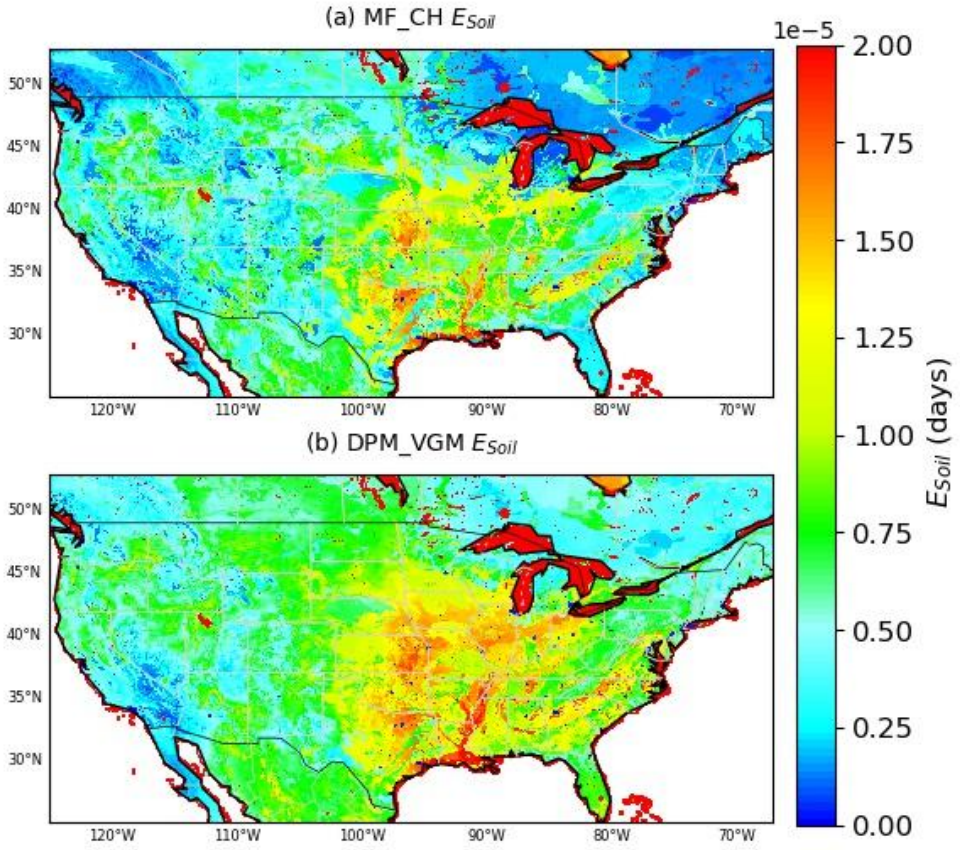

Figure S7 Spatial distribution of surface soil evaporation of (a) MF_CH; and (b) DPM_VGM.

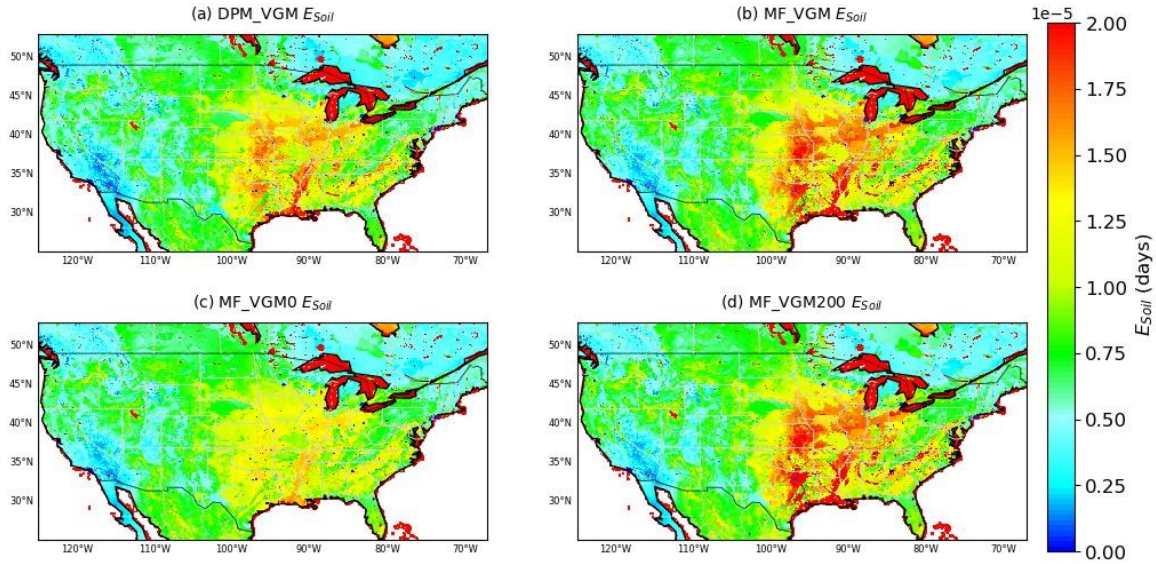

Figure S8: Spatial distribution of surface soil evaporation of (a) DPM_VGM; (b) MF_VGM; (c) MF_VGM0; and (d) MF_VGM200.